

Wide-Field Radio Transient Surveys with the Allen Telescope Array

Steve Croft*

University of California, Berkeley, 601 Campbell Hall #3411, Berkeley, CA 94720, USA

E-mail: scroft@astro.berkeley.edu

Geoff Bower

University of California, Berkeley, 601 Campbell Hall #3411, Berkeley, CA 94720, USA

The Allen Telescope Array Team

UC Berkeley Radio Astronomy Laboratory and The SETI Institute

We present the Allen Telescope Array Twenty-centimeter Survey (ATATS), a multi-epoch (12 visits), 690 square degree radio map and catalog at 1.4 GHz. The combined map using data from all epochs has RMS noise $3.94 \text{ mJy beam}^{-1}$, and dynamic range 1050, with a circular beam of $150''$ FWHM. It contains 4408 sources to a limiting sensitivity of $5\sigma = 20 \text{ mJy beam}^{-1}$. We compare the catalog generated from this map to the legacy NVSS. Our data show that we can reliably measure flux densities and positions of radio sources. We also place constraints on the population of transient radio sources in our survey field.

ISKAF2010 Science Meeting - ISKAF2010

June 10-14, 2010

Assen, the Netherlands

*Speaker.

1. Radio Transients

The radio sky is far from unchanging. Time-varying radio sources such as some stars (Güdel, 2002), pulsars (Archibald et al., 2009), microquasars (Miller-Jones et al., 2009), and AGNs (e. g. , Aller et al., 1992) — the latter making up almost all of the sources seen in imaging surveys above a few mJy at 1.4 GHz (Seymour et al., 2008) — are seen to change in brightness over a range of timescales. These are typically rotating sources, or sources with variable accretion rates or magnetic fields. Transient sources (i. e. , those with no detectable quiescent radio counterpart) typically have explosive progenitors, such as gamma ray bursts (Frail et al., 2000) and radio supernovae (Brunthaler et al., 2009) – where the progenitor is destroyed – or flares from a variety of objects, which may or may not also show up as variable sources during their more quiescent periods. Flares are seen from AGNs (Falcke et al., 1999), M-dwarfs (Jackson et al., 1989), brown dwarfs (Berger et al., 2001; Hallinan et al., 2007), pulsars (Cognard et al., 1996), and rotating radio transients (RRATs; McLaughlin et al., 2006), among other classes of object.

Sometimes transient radio sources are seen but the progenitor remains unidentified in deep imaging at other wavelengths. Bower et al. (2007) studied a deep image from 944 epochs of a VLA archival field at 5 and 8.4 GHz, spanning 22 years with a period of 7 days. They detected ten transient sources at flux densities $\lesssim 2$ mJy, eight of which were seen only in a single epoch. No counterparts were seen for six transients in deep optical and infrared imaging, and their progenitors remain unknown. Similarly, Matsumura et al. (2009) report the detection of nine transients with much larger flux densities ($\gtrsim 1$ Jy) in drift scanning observations at 1.4 GHz with the Nasu Pulsar Observatory, but with no counterparts at other wavelengths. Such sources may perhaps be flares from isolated old neutron stars (Ofek et al., 2010) or maybe something more exotic.

2. The Allen Telescope Array

The Allen Telescope Array (ATA), a joint project of the Radio Astronomy Laboratory of the University of California, Berkeley, and the SETI Institute in Mountain View, CA, is a telescope optimized for high throughput, and so it can scan large areas of sky to faint flux density limits in a short amount of time. This makes it an ideal instrument to look for time-varying and variable sources, because the high cadences permitted by the telescope design enable frequent visits to the same large area of sky to look for changes. The 42 small dishes (each 6 m in diameter) have a field of view of 5 square degrees at 1.4 GHz, much larger than the Very Large Array, although with poorer resolution ($2' \times 4'$) at this frequency.

The relatively small volumes of data produced by the previous generation of radio telescopes meant that flagging RFI, calibration, and imaging, could all practically be performed interactively. This becomes impractical for the next generation of radio telescopes, and automated routines are required to get the best results. Correlator data taken with the ATA are typically reduced using a custom suite of scripts programmed by Garrett Keating known as RAPID (Rapid Automated Processing and Imaging of Data; Keating et al., 2009). RAPID consists of csh scripts — work is underway to port these scripts to Ruby — that call MIRIAD (Sault et al., 1995) tasks. It performs identification and excision of RFI by looking for channels which deviate from long term averages (Fig. 1). It calibrates the visibilities using a primary flux calibrator, and images the individual

pointings. It then performs phase self-calibration and amplitude flagging, as well as identifying and flagging antennas and baselines which do not converge to a good solution. Imaging is performed using an “intelligent CLEAN” algorithm which iteratively increases the CLEAN depth until a maximum dynamic range is reached. With very little additional human interaction, RAPID is capable of making good quality images from raw ATA data.

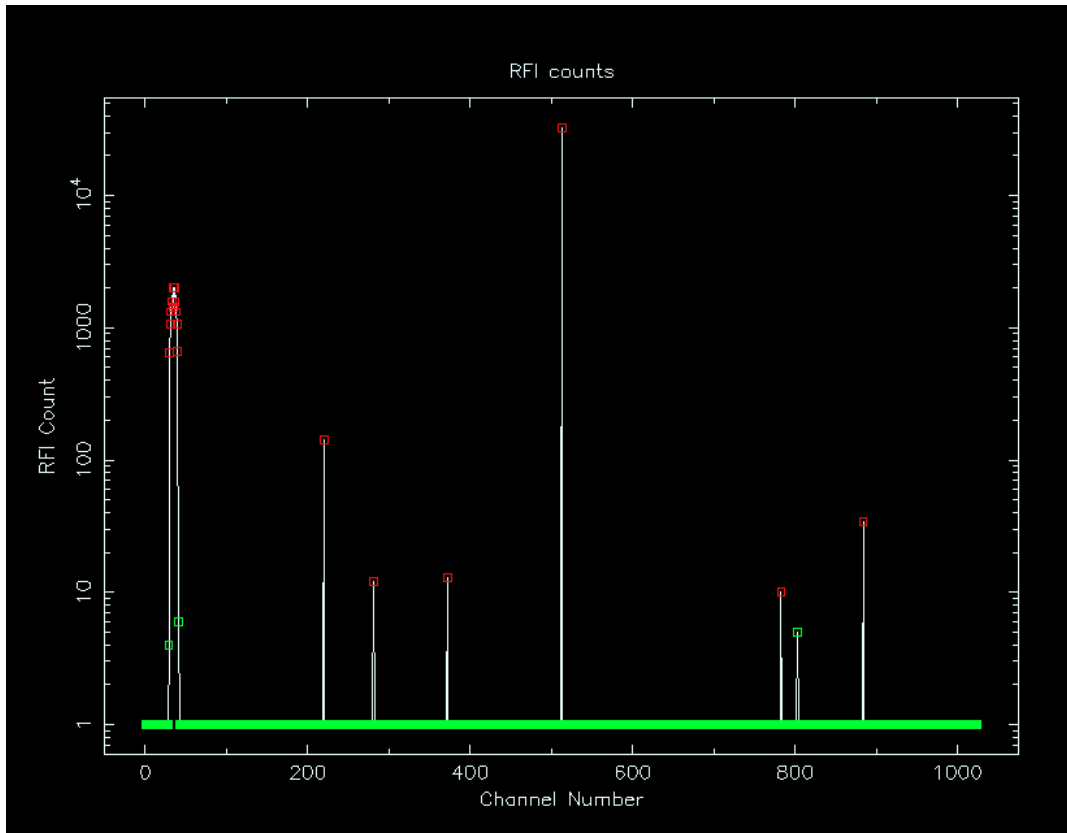


Figure 1: Screenshot from the RAPID RFI flagging program, showing RFI statistics as a function of channel. Channels with large numbers of deviant data points are flagged as likely RFI.

Mosaicking, catalog creation, and matching to legacy surveys are performed by additional custom-written scripts known as “SLOW” (Source Locator and Outburst Watcher) which create mosaic images, keeping only regions where good data exist at all epochs. SLOW uses SFIND in MIRIAD to generate catalogs, matching these across epochs and to the NRAO VLA Sky Survey (NVSS). The matched catalog is stored in an SQL database. SLOW creates postage stamps and light curves for all sources detected, and by querying the database, catalog information, postage stamps and light curves can be displayed in a web browser for the selected sample.

3. The ATA Twenty-centimeter Survey

To verify the performance of the ATA during commissioning (by comparison to existing sky survey data), as well as to search for time-varying and transient sources, we undertook the ATA

Twenty-centimeter Survey (ATATS). The survey was designed to cover large areas (~ 690 square degrees) at a comparatively low sensitivity. We observed the field 12 times over a period of three months, and produced a deep map using data from all epochs, as well as individual maps at each epoch. We present many more details of ATATS, as well as results from the comparison of the deep field with NVSS, in our recent paper, Croft et al. (2010). Analysis of epoch-to-epoch variations in ATATS will be presented in Croft et al. (2010b).

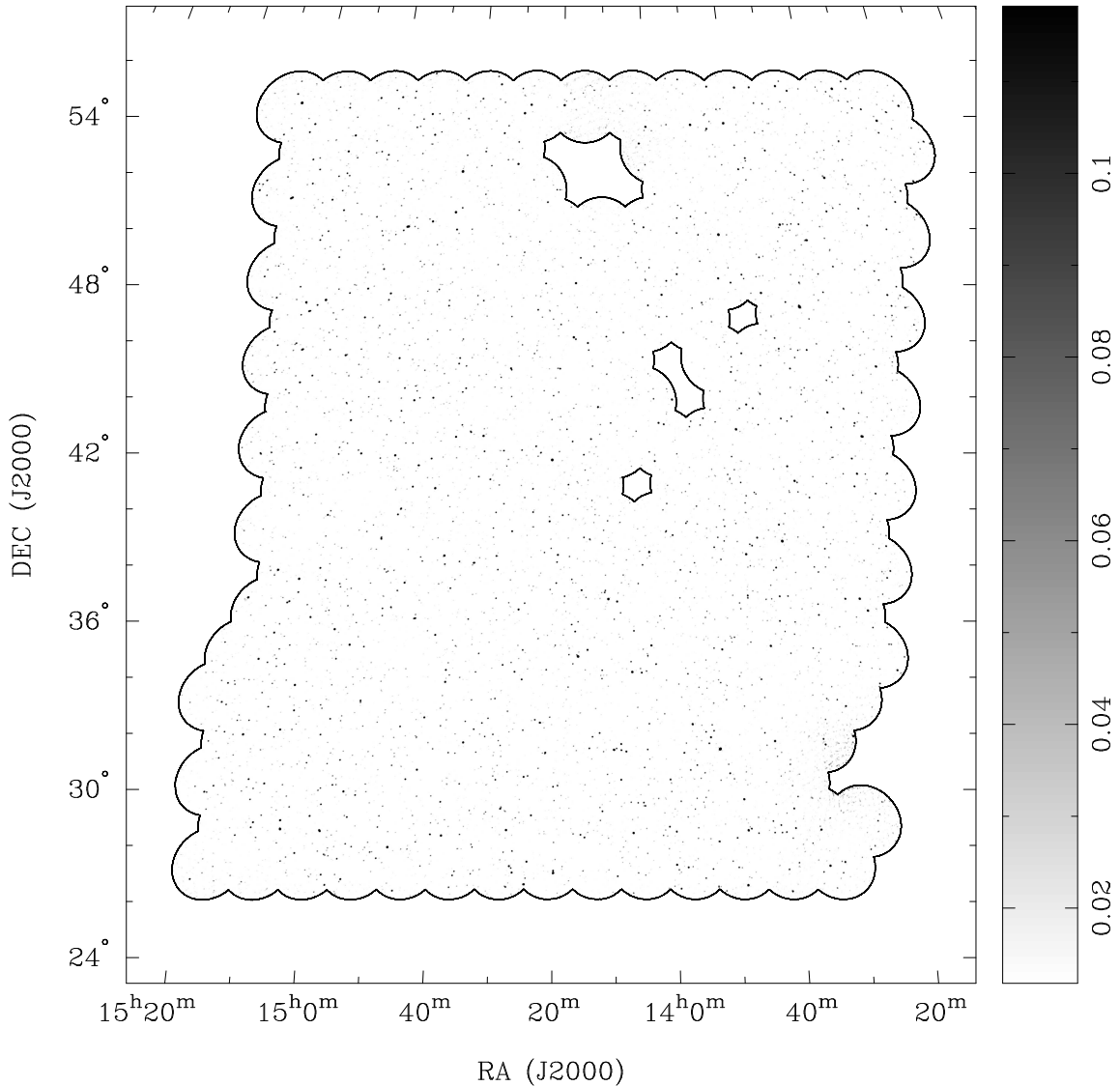
The deep map (using data from all epochs) has RMS noise $3.94 \text{ mJy beam}^{-1}$, and dynamic range 1050, with a circular beam of $150''$ FWHM. It contains 4408 sources to a limiting sensitivity of $5\sigma = 20 \text{ mJy beam}^{-1}$. A map of the deep field is shown in Fig. 2, and a section of it, with NVSS sources overplotted for comparison, is shown in Fig. 3.

We compare the flux density of the sources from the deep ATATS catalog with the sum of flux densities of all NVSS sources within $75''$ of each ATATS position in Fig. 4. Overall, the agreement is good — a least squares fit has a gradient of 1.006 ± 0.003 and an intercept of $1.3 \pm 0.5 \text{ mJy}$. Some of the scatter around the 1:1 line is due to uncertainties in the measurements of flux densities in both ATATS and NVSS, and some is due to intrinsic variability in the sources themselves over the ~ 15 years between the NVSS and ATATS observations

We can assess the completeness and reliability of ATATS by plotting the flux density distribution of our catalogs and comparing to the NVSS for the same area of sky, as in Fig. 5. The two histograms are consistent, within the errors, until the ATATS counts turn over between 40 and 80 mJy. The ATATS histogram is marginally higher than that for NVSS for the bins between 320 and 1280 mJy, and marginally lower for the bins between 40 and 160 mJy (above the points where the source counts turn over). This is to be expected since the poorer resolution of ATATS will tend to combine the flux of multi-component NVSS sources into a single brighter ATATS source, and occasionally to detect extended flux resolved out by NVSS. The ratio of the ATATS to NVSS histograms can also be interpreted as the efficiency with which we would detect transient sources of a given brightness, or as a measure of the survey completeness. We plot the ratio of the two histograms, which we denote C , in Fig. 5. ATATS is $> 90\%$ complete down to around 40 mJy, or approximately 10 times the RMS noise, below which the completeness falls off rapidly. The shift of some sources into higher flux bins due to the resolution mismatch results in some bins with computed $C > 1$.

We plot the ATATS flux density against the ATATS flux density divided by the sum of the flux densities of NVSS sources within $75''$ in Fig. 6. The scatter around the 1:1 line increases towards fainter ATATS flux densities, suggestive of increased fractional variability for fainter sources. An asymmetry in the point cloud can be seen, most obviously at flux densities fainter than the ATATS completeness limit (to the left of the dotted lines in Fig. 6). This asymmetry is due to the different resolutions and sensitivities of NVSS and ATATS. Above the completeness limit the point cloud is more symmetric about the 1:1 line, although there are still more outliers that appeared to get brighter from NVSS to ATATS than those that appeared to get fainter.

Of the 4408 ATATS sources, 4333 had a match in NVSS. Of the remaining 75 sources without an NVSS match, 39 are above 40 mJy, the ATATS 90% completeness limit. We examined postage stamp images for these 39 sources (from the ATATS mosaic and from NVSS) and concluded that none were real transient sources. In the majority of cases, these were sources which consisted of multiple NVSS sources (usually as part of a double source – presumably a radio galaxy) which



POS (I S K A F 2 0 1 0) 0 1 4

Figure 2: The deep field image, made from a combination of all 12 epochs. The solid line shows the edge of the mosaic – note that some small regions with fewer than 9 epochs of good data were not included in the mosaic. The areas near 3C 295 (the large missing region at top center) and 3C 286 (the notch cut into the lower right edge) are notable examples, but there are also a few smaller regions missing, where > 4 epochs were unusable due to RFI or some other problem. The greyscale runs from $11.82 \text{ mJy beam}^{-1} (3\sigma)$ to $118.2 \text{ mJy beam}^{-1} (30\sigma)$.

were not successfully deblended by ATATS. Examples of some of these sources are shown in Fig. 7. Similarly, 61 sources appeared to have varied by a factor of 2 or more, but had complex morphologies making it likely that the differing survey resolutions and sensitivities were responsible for the apparent variation. There were six sources which appeared compact and isolated as well as having varied by a factor of two or more. Examples of these sources are also shown in Fig. 7.

We can use the lack of transients seen when comparing ATATS to NVSS to place constraints on the population of transient sources brighter than $\sim 40 \text{ mJy}$. Fig. 8 shows the constraints on transient

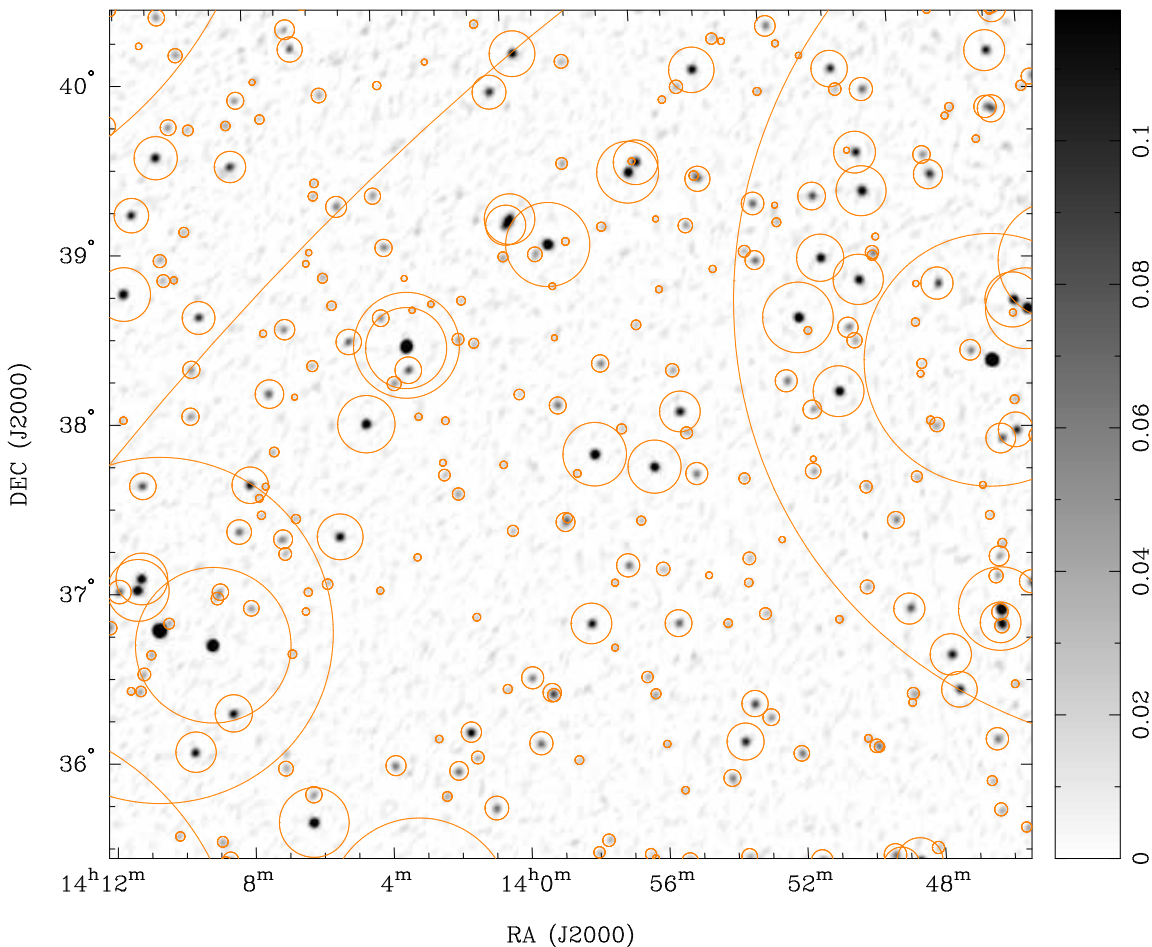


Figure 3: A 25 square degree region of the deep field shown in Fig. 2, shown at a larger scale and slightly different stretch so that the structure of individual sources may be seen. All sources with NVSS flux densities brighter than 20 mJy (corresponding to 5 times the RMS of the ATATS image) are plotted as circles; the size of the circle is proportional to the NVSS flux density. The greyscale runs from zero to 118.2 mJy beam⁻¹(30 σ). The faintest NVSS sources are below the ATATS completeness limit. Hence the fraction of NVSS sources without a counterpart in the ATATS catalog increases with decreasing circle size in this image.

rates from some surveys from the literature, compared to the constraint from the comparison of ATATS and NVSS. It is hard to reconcile the steeply falling source counts suggested by the Gal-Yam et al. (2006) and ATATS results with the detections of 9 transients brighter than 1 Jy reported by Matsumura et al. (2009) unless these transients make up a different population with a very steep cutoff below 1 Jy. The ATATS 2 σ upper limit is marginally consistent with the M09 results above 1 Jy, but if the Matsumura et al. transients have flat or rising source counts towards fluxes < 1 Jy we would expect to see them in ATATS.

Some transients may be too faint to show up in the map made from data from all epochs, but nevertheless be visible in individual epochs. To study such sources, as well as the variability of all sources from epoch to epoch, we are examining light curves and postage stamps, as shown in Fig. 9 – the results from this analysis will be discussed in Croft et al. (2010b).

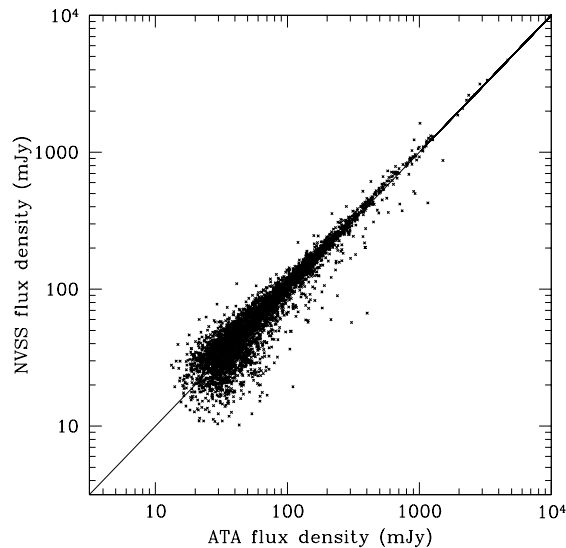


Figure 4: Comparison of the flux densities of sources from the ATATS catalog, with the sum of fluxes of all NVSS sources within $75''$ of the ATATS positions.

4. Future plans

Future plans call for an expansion of the ATA from 42 to 350 antennas, considerably increasing its survey speed. The ATA team is working in partnership with other SKA pathfinders, including LOFAR, and welcomes approaches from other parties interested in collaborating on science using the ATA, on simultaneous campaigns with other instruments, and in building the support and infrastructure necessary as we transition from telescopes with tens of elements to those with hundreds or thousands.

Acknowledgments

I acknowledge the support of the American Astronomical Society and the National Science Foundation in the form of an International Travel Grant, and the support of the conference organizers, which enabled me to attend this conference.

References

- Aller, M. F., Aller, H. D., & Hughes, P. A. 1992, *ApJ*, 399, 16
- Archibald, A. M., et al. 2009, *Science*, 324, 1411
- Berger, E., et al. 2001, *Nature*, 410, 338
- Bower, G. C., Saul, D., Bloom, J. S., Bolatto, A., Filippenko, A. V., Foley, R. J., & Perley, D. 2007, *ApJ*, 666, 346

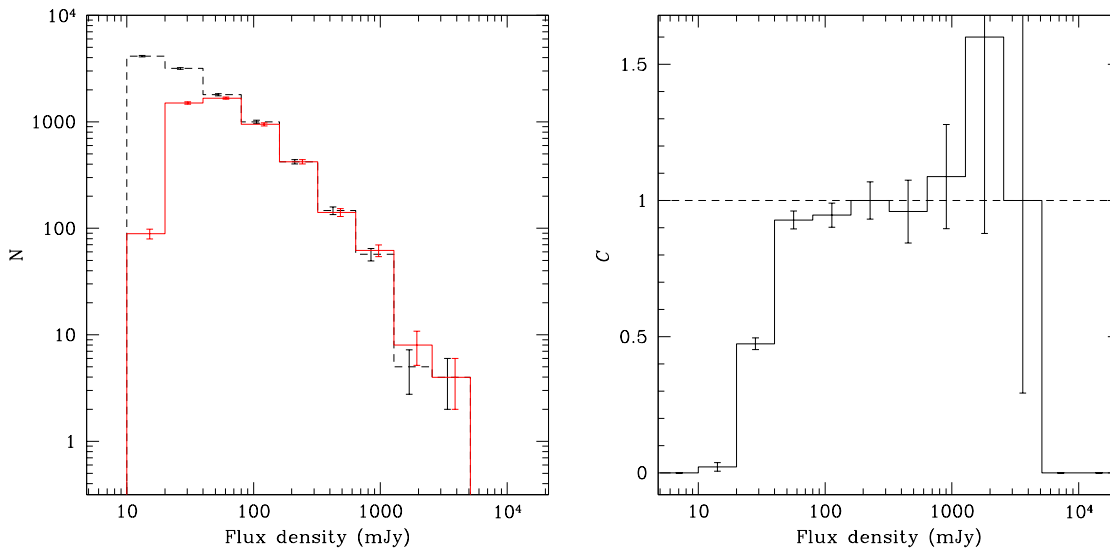


Figure 5: *Left:* Log(N) – log(S) histogram of NVSS sources brighter than 10 mJy (black dashed line) in good regions of the ATATS field, and sources detected in the ATATS catalog (red solid line) over the same area. Error bars assume Poisson statistics. Each bin covers a factor of 2 in integrated flux density, or 0.301 dex. The coarser resolution of the ATA tends to combine the flux from a tight cluster of NVSS sources into a single ATATS source. Combined with the ATA’s additional sensitivity to structures larger than the NVSS synthesized beam, this tends to shift some sources from fainter into brighter bins. *Right:* Ratio of the histograms for the ATATS and NVSS catalogs, $C = N_{\text{ATATS}}/N_{\text{NVSS}}$. This represents a measure of the completeness of the ATATS catalogs. Error bars are computed by propagating the Poisson errors from the ATATS and NVSS source count histograms. The tendency of the ATA to shift sources into higher flux bins results in some bins with $C > 1$. These bins are consistent with 100% completeness (dashed line) within the Poisson errors.

Brunthaler, A., Menten, K. M., Reid, M. J., Henkel, C., Bower, G. C., & Falcke, H. 2009, *A&A*, 499, L17

Carilli, C. L., Ivison, R. J., & Frail, D. A. 2003, *ApJ*, 590, 192

Cognard, I., Shrauner, J. A., Taylor, J. H., & Thorsett, S. E. 1996, *ApJ*, 457, L81

Croft, S., et al. 2010, *ApJ*, 719, 45

Croft, S., et al. 2010b, in prep.

Frail, D. A., Waxman, E., & Kulkarni, S. R. 2000, *ApJ*, 537, 191

Frail, D. A., Kulkarni, S. R., Berger, E., & Wieringa, M. H. 2003, *AJ*, 125, 2299

Gal-Yam, A., et al. 2006, *ApJ*, 639, 331

Güdel, M. 2002, *ARA&A*, 40, 217

Hallinan, G., et al. 2007, *ApJ*, 663, L25

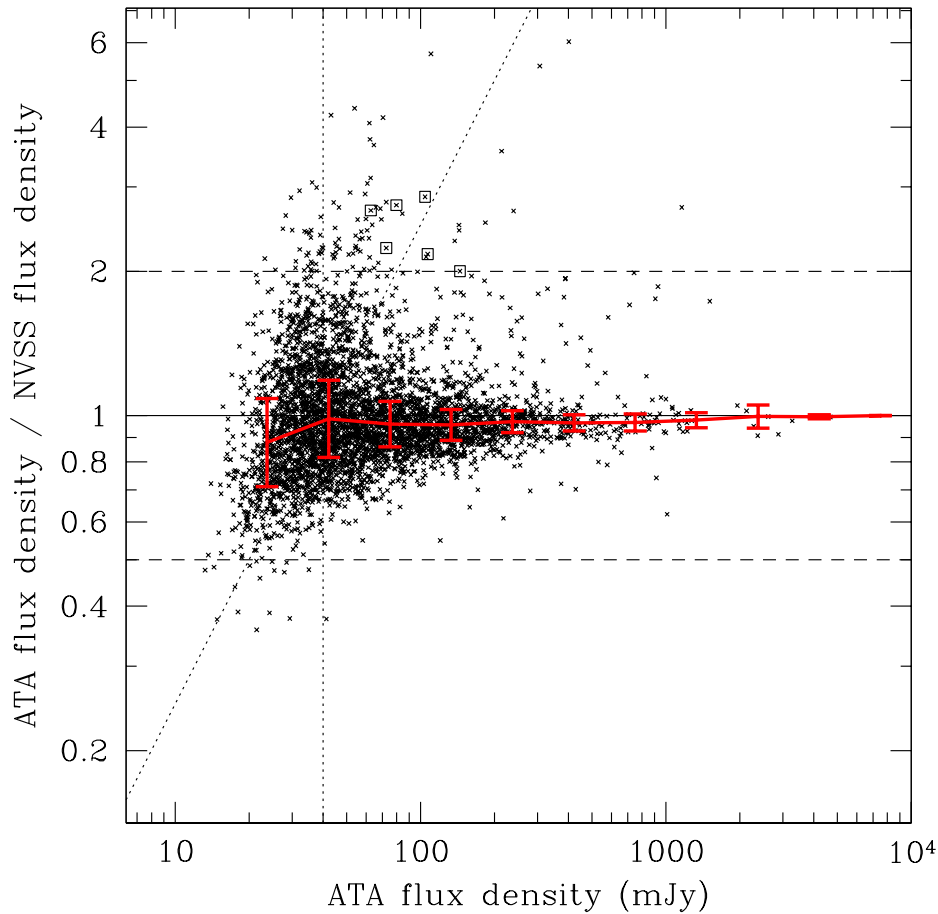


Figure 6: Comparison of the flux densities of sources from the ATATS catalog, with the sum of flux densities of all NVSS sources within $75''$ of the ATATS positions. The ratio of the ATA to NVSS flux densities is plotted as a function of ATA flux density (black crosses). Sources whose flux density does not change from the NVSS measurement to the ATATS measurement lie on the horizontal solid 1:1 line. Sources whose fluxes change by a factor of 2 lie on the horizontal dashed 1:2 and 2:1 lines. The vertical dotted line shows the ATATS completeness limit, $S_{\text{ATATS}} = 40$ mJy. The slanted dotted line shows the same limit for NVSS, $S_{\text{NVSS}} = 40$ mJy. The red solid line shows the median flux ratio in bins of 0.25 dex in S_{ATATS} , and the associated error bars show the interquartile range of the flux density ratio. We plot (as crosses enclosed by squares) the 6 sources above the ATATS completeness limit (vertical dotted line) which varied by a factor of 2 or more and which appeared relatively compact and isolated in both the ATATS and NVSS images.

Falcke, H., et al. 1999, ApJ, 514, L17

Jackson, P. D., Kundu, M. R., & White, S. M. 1989, A&A, 210, 284

Keating, G., Barott, J., & Allen Telescope Array Team 2009, American Astronomical Society Meeting Abstracts, 214, #601.06

Matsumura, N., et al. 2009, AJ, 138, 787

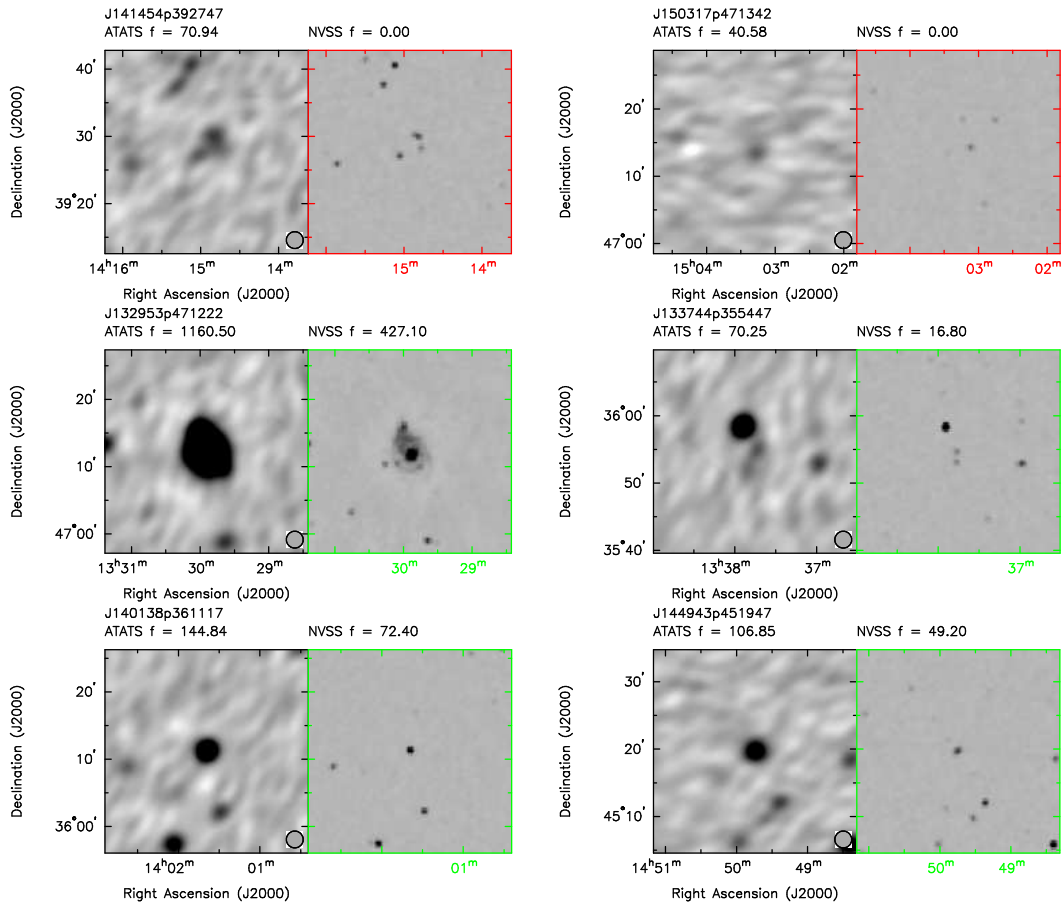


Figure 7: *Top row:* Examples of some of the 39 transient candidates with $S_{\text{ATATS}} \geq 40$ mJy and $S_{\text{NVSS}} = 0$. None are truly transients. *Middle row:* Examples of some of the 61 candidates that appeared to have varied by more than a factor 2 in flux density from NVSS to ATATS, but have complex morphologies. Such sources are prone to resolution effects and less likely to be truly highly variable than are isolated sources. *Bottom row:* Two of the six sources which we judged good candidates (i.e., those which appear compact and isolated, and are brighter than the ATATS completeness limit) to have varied by more than a factor 2 in flux density from NVSS to ATATS.

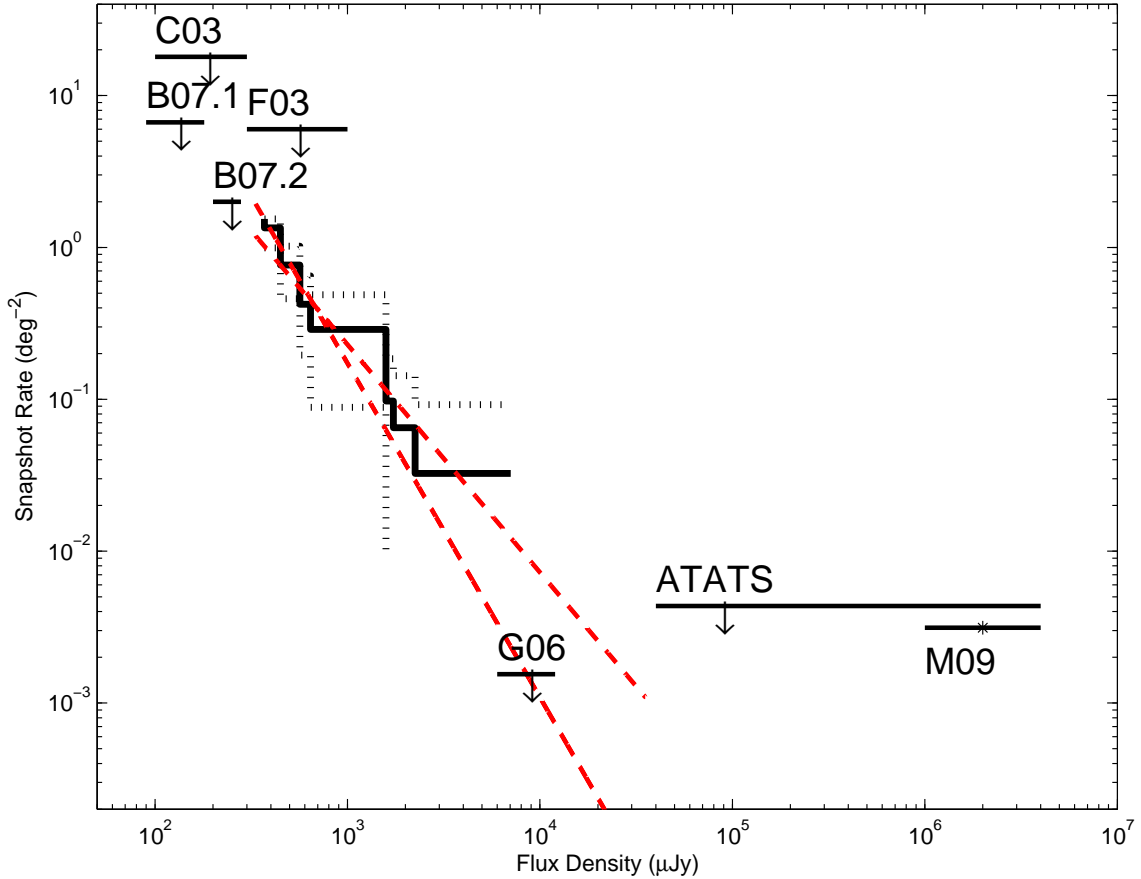
McLaughlin, M. A., et al. 2006, Nature, 439, 817

Miller-Jones, J. C. A. et al. 2009, MNRAS, 394, 309

Ofek, E. O., Breslauer, B., Gal-Yam, A., Frail, D., Kasliwal, M. M., Kulkarni, S. R., & Waxman, E. 2010, ApJ, 711, 517

Sault, R. J., Teuben, P. J., & Wright, M. C. H. 1995, Astronomical Data Analysis Software and Systems IV, 77, 433

Seymour, N., et al. 2008, MNRAS, 386, 1695



POS (I S K A F 2 0 1 0) 0 1 4

Figure 8: Cumulative two-epoch source density for radio transients as a function of flux density, based on Fig. 9 of Bower et al. (2007). The solid black line shows the rate measured for transients with characteristic timescales < 7 days from Bower et al. (2007), while the broken black lines show the 2σ upper and lower bounds. The red dashed lines show $S^{-1.5}$ and $S^{-2.2}$ curves. The arrows show 2σ upper limits for transients from Bower et al. with a 1 yr timescale (labeled B07.1) and a 2 month timescale (labeled B07.2), and for transients from the comparison of the 1.4 GHz NVSS and FIRST surveys by Gal-Yam et al. (2006), labeled G06; from the Carilli et al. (2003) survey (labeled C03); from the Frail et al. (2003) survey (labeled F03); and from the Matsumura et al. (2009) survey (labeled M09). The upper limits from ATATS are only marginally consistent with the Matsumura et al. detections. Constraints from data from individual ATATS epochs will be discussed in Croft et al. (2010b).

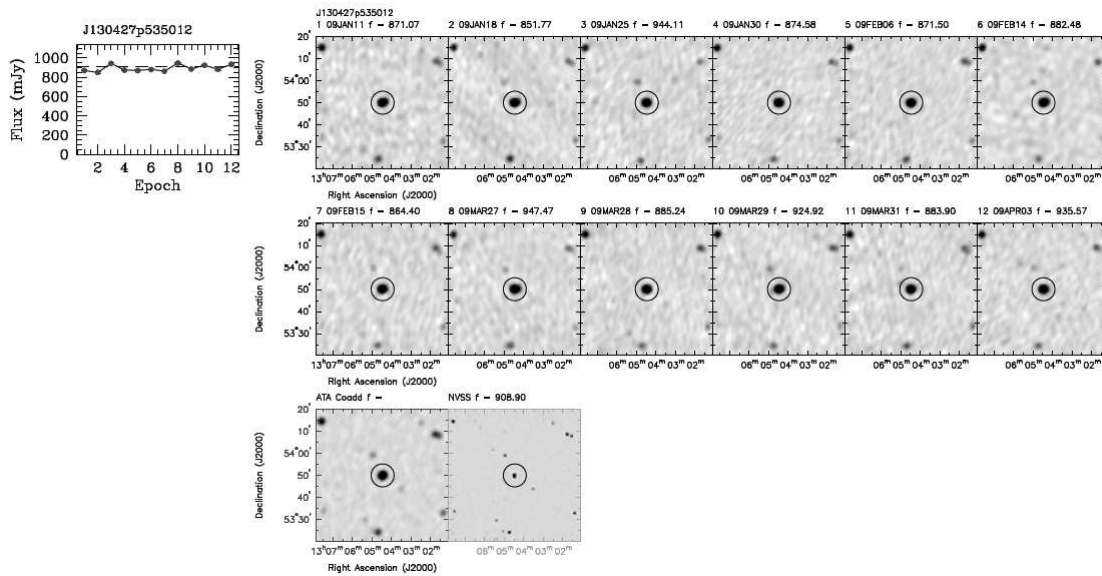


Figure 9: Lightcurve and postage stamps for a bright ATATS source, as produced by the SLOW pipeline.